Biomechanics and Modeling in Mechanobiology
https://doi.org/10.1007/s10237-018-1038-3

ORIGINAL PAPER

A nonlinear homogenized finite element analysis of the primary stability of the bone–implant interface

Marzieh Ovesy[1] · **Benjamin Voumard**[1] · **Philippe Zysset**[1]

Received: 19 March 2018 / Accepted: 22 May 2018
© Springer-Verlag GmbH Germany, part of Springer Nature 2018

Abstract
Stability of an implant is defined by its ability to undergo physiological loading–unloading cycles without showing excessive tissue damage and micromotions at the interface. Distinction is usually made between the immediate primary stability and the long-term, secondary stability resulting from the biological healing process. The aim of this research is to numerically investigate the effect of initial implantation press-fit, bone yielding, densification and friction at the interface on the primary stability of a simple bone–implant system subjected to loading–unloading cycles. In order to achieve this goal, human trabecular bone was modeled as a continuous, elasto-plastic tissue with damage and densification, which material constants depend on bone volume fraction and fabric. Implantation press-fit related damage in the bone was simulated by expanding the drilled hole to the outer contour of the implant. The bone–implant interface was then modeled with unilateral contact with friction. The implant was modeled as a rigid body and was subjected to increasing off-axis loading cycles. This modeling approach is able to capture the experimentally observed primary stability in terms of initial stiffness, ultimate force and progression of damage. In addition, it is able to quantify the micromotions around the implant relevant for bone healing and osseointegration. In conclusion, the computationally efficient modeling approach used in this study provides a realistic structural response of the bone–implant interface and represents a powerful tool to explore implant design, implantation press-fit and the resulting risk of implant failure under physiological loading.

Keywords Bone–implant interface · Primary stability · Finite element modeling · Damage · Contact · Press-fit · Friction

1 Introduction

The mechanical stability of an implant is defined as its ability to sustain cyclic loading without producing excessive damage in the bone and undergoing excessive micromotions at the interface. The overall mechanical stability can be divided into primary and secondary stability. Primary stability is defined at the time of implantation and is related to the peripheral bone volume fraction, the orientation of the trabeculae and the contact condition between the implant and bone (Zhang et al. 2004; Lioubavina-Hack et al. 2006; Ruffoni et al. 2012; Basler et al. 2013), whereas secondary stability is defined after the biological process of healing and modeling of the bone leading to osseointegration and improved load transfer between bone and implant (Meredith 2008; Chappuis et al. 2013; Haïat et al. 2014).

For small motions associated with small loads, the extent of primary stability is mainly characterized by stiffness of the bone–implant system, while for higher motions associated with larger loads, the ultimate force supported by the bone–implant system becomes the dominant characteristic of this stability. From a clinical stand point, this ultimate load defines a threshold above which the implant drifts irreversibly within the bone.

An enhanced primary stability allows for immediate loading of the implant and may save a second intervention for mounting the crown after bone healing around the implant (Gapski et al. 2003; Steiner et al. 2015). A better understanding and an accurate estimation of primary stability are therefore necessary to improve implant design and decide upon immediate loading at the time of first intervention.

In order to improve primary fixation, implants are usually inserted in the bone through a press-fit procedure where the drilled hole is undersized with respect to the implant. How-

✉ Marzieh Ovesy
marzieh.ovesy@istb.unibe.ch

[1] Institute for Surgical Technology and Biomechanics, University of Bern, Stauffacherstr. 78, 3014 Bern, Switzerland

Published online: 01 June 2018

ever, an excessive press-fit may induce damage in the bone, decrease primary stability and even lead to implant loosening. Accordingly, the amount of press-fit has remained a challenge for dentists.

As a result, experimental and numerical techniques have been developed in order to investigate the extent of primary stability (Abdul-Kadir et al. 2008; Chong et al. 2010; Conlisk et al. 2012; Berahmani et al. 2017). The experimental approaches consist of mechanical tests such as pull-out test in combination with imaging in order to quantify directly the amount of micromotions around the implant (Lioubavina-Hack et al. 2006; Gabet et al. 2010; Basler et al. 2013; Mueller et al. 2013; Du et al. 2015). Subtraction of micro-computed tomography (μCT) images before and after implantation reveals regions with high plastic strains and substantial damage (Steiner et al. 2016).

The numerical studies of primary stability can be divided into micro-finite element (μFE) models and homogenized finite element (hFE) models. In μFE, high-resolution μCT images are converted into voxel-based models that represent isotropic bone tissue (Rietbergen et al. 1995). The damage induced by the implantation procedure can be accounted for by the reduction in the elastic material properties at a specific boundary layer around the implant (Steiner et al. 2016, 2017a, b). The stiffness of the bone–implant system is then computed for arbitrary loading directions. In this type of analysis, the interface of bone and implant is considered to be fully bonded without the existence of contact mechanism and relative micromotions.

Although the continuum approaches model the bone as a continuous material without considering the microarchitecture, they can account for the material nonlinearity and the contact boundary conditions between bone and implant. Nonlinear behavior of the bone in large strains has been modeled as an elasto-plastic material with various yield criteria showing also damage based on the accumulated plastic strain (Charlebois et al. 2010; Hosseini et al. 2012; Schwiedrzik et al. 2013; Hosseini et al. 2014). The interface in this approach has been modeled either as fully bonded or using contact with friction (Viceconti et al. 2000; Pankaj 2013). In the fully bonded models, the μCT images with implants are converted directly into elements and micromotions between the bone and implant are neglected (Baggi et al. 2008; Fouad 2010; Karunratanakul et al. 2010). Micromotions come into account when the assumption of unilateral contact between the bone and implant is made. In this case, two categories of simulations exist. First, the models do not account for the pre-implant stress by considering the bone to be intact at the time of loading (MacLeod et al. 2012; Dorogoy et al. 2017; Korabi et al. 2017) and the models induce the stress generated during the implantation procedure either through a prestress configuration (Inzana et al. 2016; Varga et al. 2017) or through motion of the boundaries in order to mimic the press-fit situation (Berahmani et al. 2017).

In summary, despite the detailed bone microstructure inherent to μFE models, they are not able to predict the primary stability of implants in terms of unloading stiffness, ultimate force and micromotions, which is mainly due to the lack of contact condition and the restriction to elastic bone properties. On the other hand, current hFE models either do not account for implantation damage or consider the interface as fully bonded.

Accordingly, the aim of the present study is to develop, characterize and validate an efficient hFE model for the primary stability of a cylindrical implant subjected to cyclic loading after a press-fit fixation in homogeneous trabecular bone. The effect of different modeling parameters such as the initial amount of press-fit, interface contact definition and friction on stiffness and ultimate force is quantified. A mesh convergence analysis is also performed. Finally, the predictions of the hFE model are compared to a recent cyclic loading experiment of a dental implant. The summary of the study is presented in Fig. 1.

2 Materials and methods

2.1 Model geometry and mesh

Homogeneous trabecular bone cylinders of 13 mm diameter and 19 mm length embedded in poly (methyl methacrylate) (PMMA) are considered for implant fixation. The implant geometry was simplified by ignoring the threads and modeled as a cylinder mimicking the outer dimensions of the NobelActive implant (3.5 mm $\times$ 13.0 mm) from Nobel Biocare. The implant is placed in the bone by first removing a hole in the bone and later inserting the implant through a radial press-fit procedure inside the trabecular bone cylinder in order to assure the full contact between the two bodies. In clinical practice, the diameter of the drilled hole is selected based on bone density. In this study, the drilling diameters used for soft ($\phi = 2$ mm) and dense ($\phi = 3.2$ mm) bone were chosen and named the soft and dense protocol, respectively. In addition, an intact protocol was also defined and studied where the drilled hole had exactly the same diameter as the implant ($\phi = 3.5$ mm). The trabecular bone cylinder was meshed with 7776 linear hexahedral elements of type C3D8 (Fig. 4). The region around the drilled hole was meshed with small elements of seed size 0.2 mm, and the seed size increased to 1.5 mm at the outer diameter.

2.2 Material modeling

The homogenized finite element method is used in this study. Due to the high difference in stiffness, the implant was

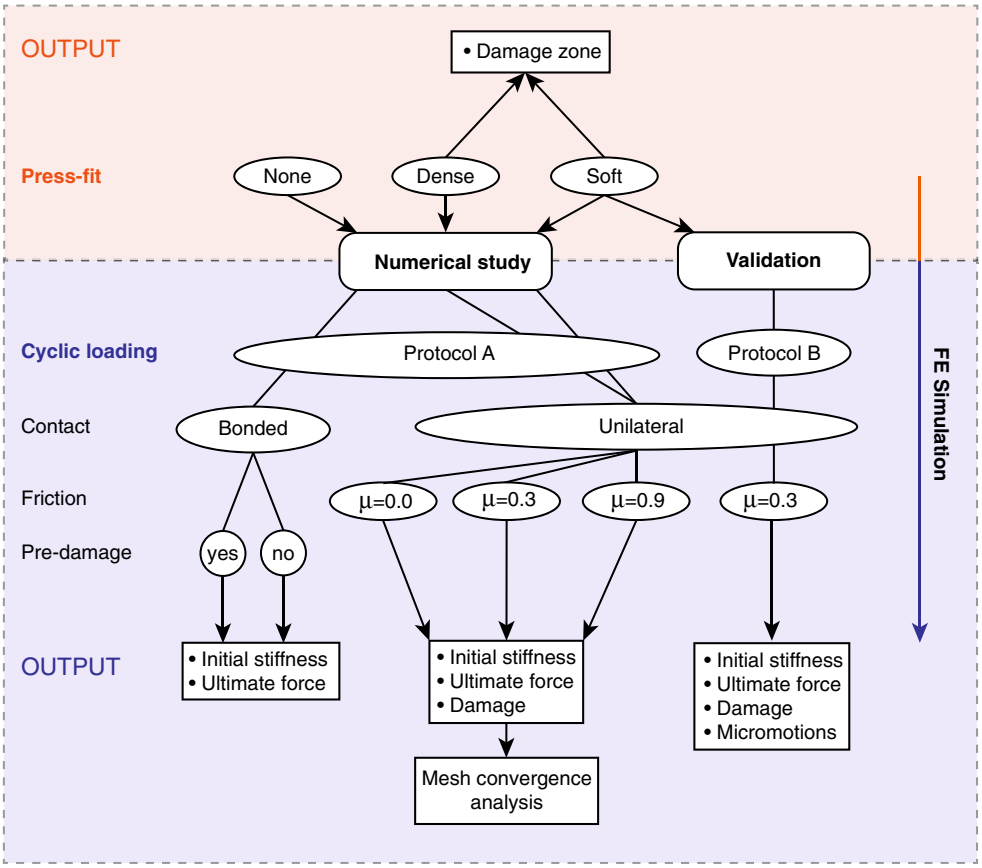

Fig. 1 The summary of the tasks performed throughout this study

considered as a rigid body compared to the bone. As for trabecular bone, a constitutive model that accounts for the nonlinear behavior in large strains was chosen and applied in the finite element package Abaqus (Abaqus 6.14 Dassault Systems, France) using a user material subroutine (UMAT) (Charlebois et al. 2010; Hosseini et al. 2012; Schwiedrzik et al. 2013). This model simulates the behavior of an elasto-plastic orthotropic material with a quadric yield surface, whose parameters depend on bone volume fraction (BV/TV) and the trabecular orientation described by a fabric tensor. The post-yield behavior is modeled without hardening or softening, but with densification that represents the progressive collapse and compaction of the trabeculae (Charlebois et al. 2010). The densification is triggered when the volumetric strain of the material has reached a large strain threshold and is modeled as the superposition of a linear and a nonlinear spring. The function and values used for the densification behavior are reported in Table 1 (Hosseini et al. 2015). The damage is also introduced through the material definition by reducing the stiffness with a certain amount $(1 - D)$, where D is an exponential function starting from zero in the absence of plastic strains, reaching a maximum level of damage ($D_c = 0.86$) based on the dimensionless material

Table 1 The densification parameters (Hosseini et al. 2015)

γ_{l0} (MPa)	r_l (–)	γ_{p0} (MPa)	r_p (–)	h (–)	E_v^d (MPa)
660.0	2.928	65.0	2.77	6.0	−0.2

constant ($a = 8.0075$) and cumulative plastic strain (κ) in the material as mentioned in Eq. 1 (Wolfram et al. 2011).

$$D_\kappa = D_c(1 - e^{-a\kappa}) \tag{1}$$

A constant value of BV/TV was assigned to 10.9%, and the values of 1.46, 0.77 and 0.77 were attributed to the three eigenvalues of the fabric tensor with the eigenvector with the largest eigenvalue oriented along the axis of the implant. As the effect of boundary conditions at the interface resembles better the periodic mixed uniform boundary condition (PMUBC), the mechanical and post-yield properties of the bone were chosen to be equal to the values reported by Panyasantisuk et al. (2016) indicated in Table 2.

Table 2 Fabric-based transversely isotropic bone material properties (Panyasantisuk et al. 2016)

ϵ_0 (MPa)	ν_0 (–)	μ_0 (MPa)	k (–)	δ (–)	l (–)	
9759	0.2289	3117	1.91	1.0	1.10	
σ_0^+ (MPa)	σ_0^- (MPa)	ζ_0 (MPa)	τ_0 (MPa)	p (–)	δ (–)	q (–)
57.69	73.10	0.280	29.61	1.82	1.00	0.98

2.3 Interface modeling

The interface was modeled using unilateral contact, but a comparison was made with the fully bonded approach. For the first approach, the contact at the interface was defined through a separable surface to surface contact definition. Normal contact in combination with friction acting in the tangential direction was considered in the model. The friction coefficient was varied from 0 (no friction) to 0.9 according to the values reported in the literature, and the slip tolerance of 0.05 was used (Dorogoy et al. 2017). In the second approach, the boundaries of the implant were assumed to be fully bonded to the surrounding bone. In published fully bonded models, the bone is assumed to be purely elastic and the implantation damage is applied by a reduction in Young's modulus at a certain vicinity of the implant (Steiner et al. 2017b). Accordingly, two fully bonded elastic simulations, one without damaged zone (FBNDZ) and one with a damaged zone (FBWDZ), were performed. In the second simulation, a radius of 0.3 mm around the implant had damage D, i.e., a reduction in Young's modulus, of 70% (Steiner et al. 2017b).

2.4 Boundary conditions and loading

The outer diameter and the bottom of the trabecular bone cylinder were fixed in three directions. The FE analysis is divided into two parts: the implantation and the cyclic loading protocol. The first was simulated by forcing the boundaries of the drilled hole to reach the boundaries of the implant. That is a radial displacement of 0.75, 0.15 and 0 mm for soft, dense and intact protocols, respectively. The cyclic loading protocol consisted of a displacement applied on a reference node in the vertical direction (z). The reference node was located 8.5 mm above and kinematically coupled to the implant as illustrated in Fig. 2a. The displacement followed the protocol shown in Fig. 2b with the reference node moving 0.04, 0.08, 0.16 and 0.32 mm as the maximum displacement of each cycle in the z direction and being free to move in the two other directions. The unloading was carried out by bringing the node back to the initial z value. Numerical convergence was verified in both implantation and loading conditions with different element seed sizes of 0.1–0.8 mm around the drilled hole.

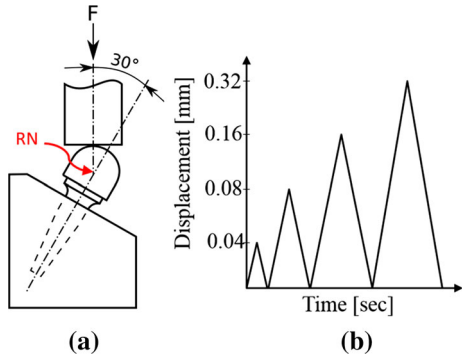

Fig. 2 Protocol A: **a** The simulated loading configuration of the implant with the implant reference node (RN). **b** The applied loading–unloading protocol

2.5 Experiment

An experiment was previously conducted in our laboratory on fifty-five samples of trabecular bone from human vertebral bodies with a BV/TV range of 6.77–16.85% and degree of anisotropy range (DA = maximum eigenvalue/minimum eigenvalue) of 1.45–2.63. The experiment was also performed on twenty-five bovine trabecular samples with a BV/TV range of 15.04–47.72% and a DA range of 1.31–2.51. In this experiment, the titanium implant was inserted using the soft or dense protocol, an abutment was screwed into the implant, and a hemispherical cup mimicking the crown was fixed on the abutment Fig. 3a. A cyclic loading–unloading protocol in the vertical direction according to Fig. 3a was applied to the cup. Each cycle was repeated three times using the approach that samples were loaded to the maximum displacement amplitude of 0.04, 0.08, 0.16 and 0.32 mm and unloaded till the reaction force in the implant reached zero (Fig. 3b). The human experimental median values for initial stiffness, ultimate force and last cycle damage are reported in Table 3.

3 Results

3.1 Implant insertion analysis

Both soft and dense protocols are simulated in the implantation process, and the amount of damage around the implant is illustrated for both cases in Fig. 4. The radius to which dam-

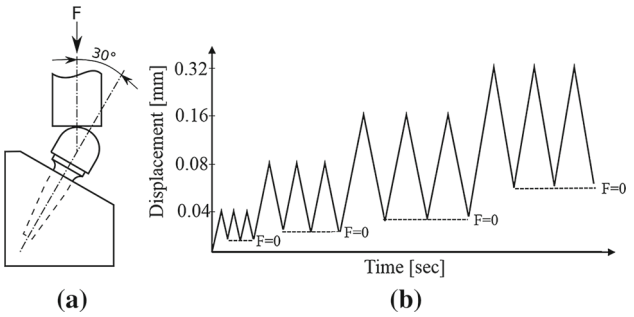

Fig. 3 Protocol B: **a** The experimental loading configuration of the implant. **b** The experimental loading–unloading protocol

Table 3 The initial stiffness (IS), ultimate force (UF) and damage parameter of soft, dense, intact, FBNDZ and FBWDZ in addition to the experiment (Exp.) results

	IS $\left(\frac{\text{N}}{\text{mm}}\right)$	UF (N)	Last cycle $(1-D)$ (–)
Soft			
$\mu = 0$	229	23	0.8
$\mu = 0.3$	432	31	0.7
$\mu = 0.9$	442	34	0.8
Dense			
$\mu = 0$	320	23	0.6
$\mu = 0.3$	566	30	0.5
$\mu = 0.9$	614	36	0.6
Intact			
$\mu = 0$	665	26	0.5
$\mu = 0.3$	904	33	0.5
$\mu = 0.9$	1044	39	0.5
Exp. soft	500	32	0.6
Exp. dense	550	28	0.6
FBNDZ	1038	332	
FBWDZ	892	285	

age extends around the middle part of the implant (plane P–P in Fig. 4 with distance 6.5 mm from the top of the implant) is approximately 1 and 2/3 mm for soft and dense protocols, respectively. In addition, the soft protocol corresponding to the higher press-fit induces an elevation of the bone surface along the periphery of the implant.

3.2 Cyclic loading

The force–displacement curves of the cyclic loading for the soft and dense drilling protocol are shown in Fig. 5 for a friction coefficient of 0.3 (Inzana et al. 2016). As a convention in this paper, the positive force represents compression and all the force–displacement curves are reported for the vertical force (F_z) and vertical displacement (U_z) of the implant reference node. As the amount of the initial induced press-

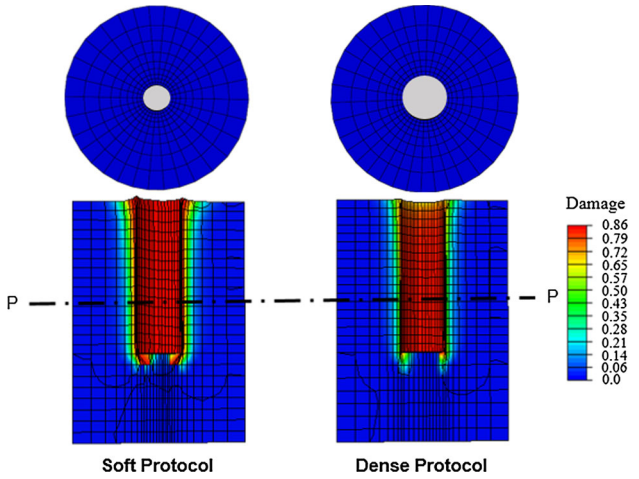

Fig. 4 Top left: the soft protocol 2 mm diameter drilled hole. Top right: the dense protocol 3.2 mm diameter drilled hole. Bottom: the implantation damage distribution for soft (left) and dense (right) protocols. Red illustrates maximum damage (0.86) and blue no damage (0)

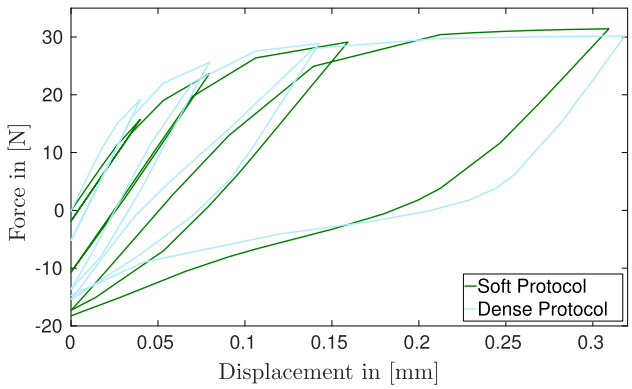

Fig. 5 The implant (RN) force–displacement curve for soft (green) and dense (blue) protocols in the cyclic loading–unloading protocol A

fit decreases, the initial stiffness increases: 432, 566 and 904 N/mm for soft, dense and intact protocols, respectively. However, the value of the ultimate force is not significantly affected by the initial implantation procedure. The value of 1-D defined as the ratio of the stiffness of the last to the first cycle is maximum for the soft protocol (Table 3). In other words, more damage occurs during the loading cycles when starting with no press-fit or with the moderate press-fit of the dense protocol.

3.3 Friction analysis

The effect of friction on the response of the bone–implant system to cyclic loading is investigated for three friction coefficients of $\mu = 0$, $\mu = 0.3$ and $\mu = 0.9$. The corresponding force–displacement curves are illustrated in Fig. 6 in the case of the dense press-fit. The initial stiffness increases from 320 to 614 N/mm and ultimate force from 23 to 36 N

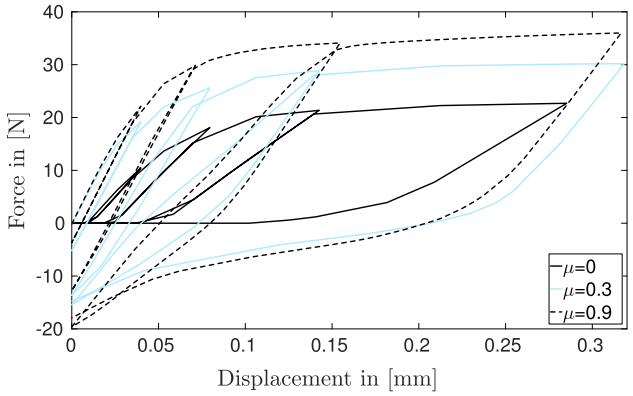

Fig. 6 Friction effect on implant (RN) force–displacement curve for dense drilling protocol followed by the cyclic loading–unloading protocol A (black: no friction, blue: $\mu = 0.3$ and dashed black: $\mu = 0.9$)

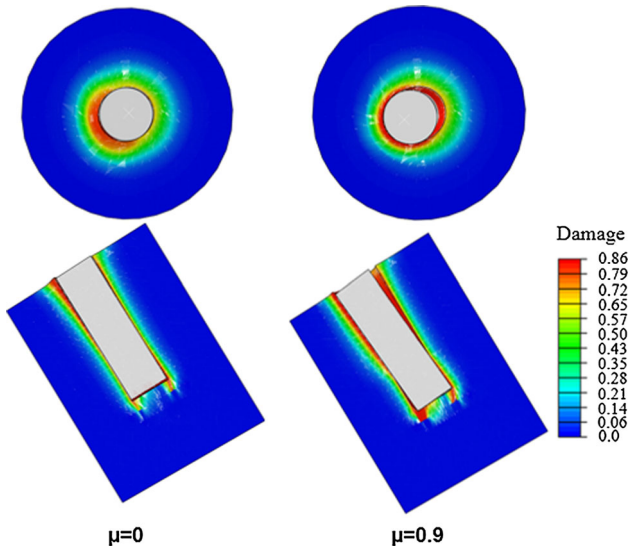

Fig. 7 Friction effect on the damage induced in the bone at the final stage of the loading–unloading cycles. Left figures: top and midsection views of $\mu = 0$. Right figures: top and midsection views of $\mu = 0.9$. Red illustrates maximum damage (0.86) and blue no damage (0)

when increasing μ from 0 to 0.9. However, the rise in initial stiffness reduces drastically from 76% for the increase of μ from 0 to 0.3 to the increase of from 0.3 to 0.9. It is also shown that when friction is accounted for, the return of the reference node to the original position produces tensile (negative) force. The midsection representations of the implant position and the related damage zone around the implant after the cyclic loading in the dense protocol for values $\mu = 0$ and $\mu = 0.9$ are shown in Fig. 7. More damage is observed in the presence of friction, especially on the superior dorsal side of the implant.

3.4 Role of a priori damage in the absence of contact

The force–displacement curves obtained with a linear elastic bone in the absence of contact but with or without a priori account of implantation-induced damage are compared in Fig. 8 with the one obtained with nonlinear bone in the presence of contact with friction ($\mu = 0.3$) and following an implantation with the dense drilling protocol. They both demonstrate a linear response of the bone–implant system where the stiffness response of FBWDZ is lower compared to FBNDZ due to the decrease in the elastic material properties in the damaged zone. In turn, stiffness for FBWDZ and FBNDZ is more than 58 and 79% higher than those obtained with the nonlinear model, respectively.

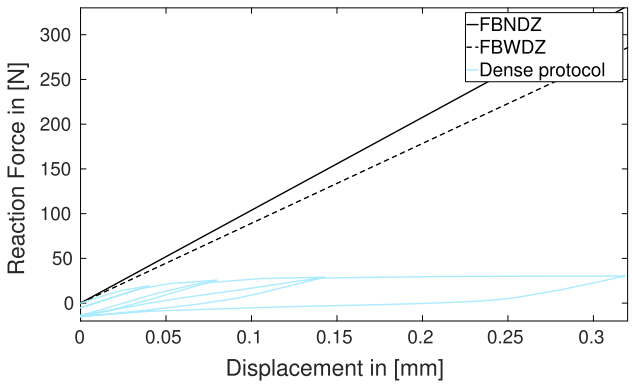

Fig. 8 Force–displacement comparison of fully bonded models and simulated dense protocol with $\mu = 0.3$ in cyclic loading–unloading protocol A (black: FBNDZ, dashed black: FBWDZ and blue: dense protocol)

3.5 Model validation

The soft protocol with friction 0.3 is simulated for four cycles up to a maximum displacement amplitude of 0.04, 0.08, 0.16 and 0.32 mm. The unloading is performed until the zero reaction force on the implant is reached. The force–displacement curve of the simulated model using the median value for the BV/TV and DA of the experiment is reported in Fig. 9 in addition to the experimental curve for a sample with a BT/TV of 11%, the closest value to the median value of the reported data. The initial stiffness of the simulation is 12% less than the experiment and the ultimate force 22% higher. As shown in Table 3, the relative stiffness reduction $(1 - D)$ for the last cycle is approximately the same in simulation and experiment. The same cyclic loading protocol B was applied to three additional values of BV/TV in order to achieve a better insight onto the effect of BV/TV on the initial stiffness and ultimate force values. The BV/TV values tested were 6.8, 10.9, 30.8 and 47.7%, corresponding to the minimum and median of the human and the median and maximum of the bovine samples, respectively. The simulation results and the regression lines fitted to the experimental values are illustrated in Fig. 10 for both initial stiffness (IS) and ultimate force (UF).

The values of initial stiffness, ultimate load and damage parameter $(1 - D)$ for the last cycle of the three protocols

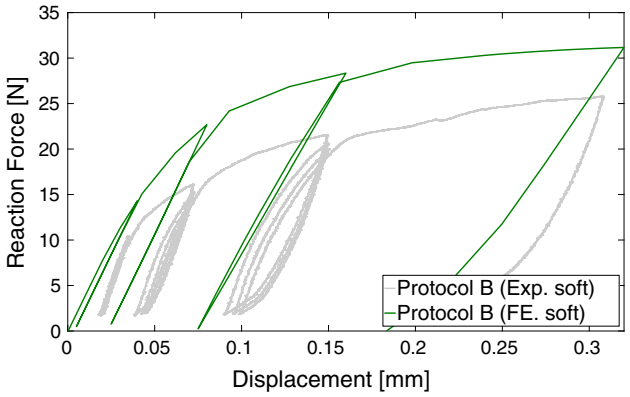

Fig. 9 Force–displacement curves for soft drilling protocol followed by the cyclic loading–unloading protocol B: the experiment (gray) versus the finite element simulation with $\mu = 0.3$ (green)

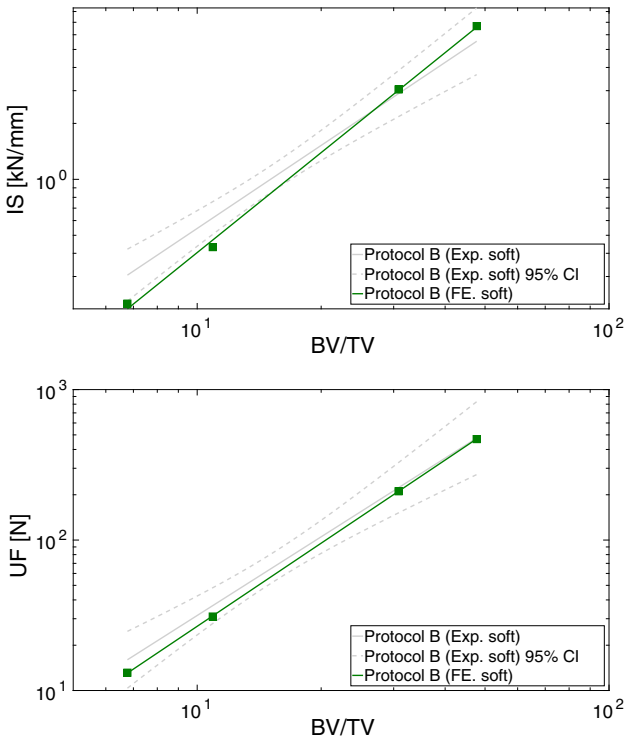

Fig. 10 Initial stiffness (IS, top) and ultimate force (UF, bottom) dependency with respect to BV/TV for the soft drilling protocol followed by the cyclic loading–unloading protocol B: regression of the experimental data (gray) with 95% confidence intervals (CI, dashed gray) versus the finite element simulation (green)

of soft, dense and intact in addition to the two fully bonded strategies are reported in Table 3. The results suggest that the change in implantation protocol from soft to intact would increase the initial stiffness and decrease the damage parameter $(1-D)$ of the model. The former is due to more damaged elements at the implantation procedure, and the latter could be explained as the less extension of damage in the presence of higher number of fully damaged elements. The ultimate force is not significantly affected by the implantation procedure.

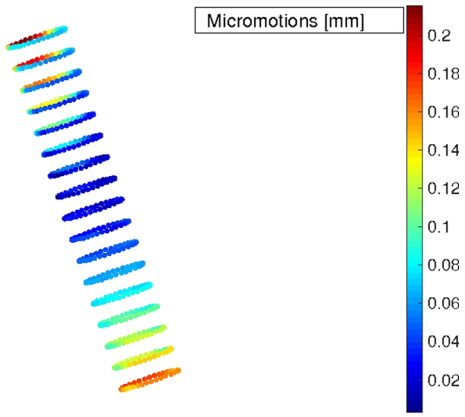

Fig. 11 Elastic micromotions in mm at the bone–implant interface during the last unloading cycle of the soft protocol with $\mu = 0.3$

Table 4 Initial stiffness (IS) and ultimate force (UF) values for mesh convergence analysis performed on soft protocol with $\mu = 0$

Seed size	IS $\left(\frac{\text{N}}{\text{mm}}\right)$	UF (N)	Last cycle $(1-D)$ (–)
0.1	228.7	23.47	0.8
0.2	229.0	23.51	0.8
0.8	234.9	24.4	0.8

3.6 Micromotions

As an illustration, the implant elastic micromotions with respect to the bone are extracted for the entire bone–implant interface. The last unloading cycle of the protocol is chosen. The beginning and the end of the specified cycle are named (A) and (B), respectively. The rigid body motion of the implant was applied to the bone nodes at the boundary and subtracted from the actual position of the respective nodes at the A and B configurations. The magnitude of the difference between the values extracted from A and B configurations is reported as micromotions in Fig. 11.

3.7 Convergence analysis

As mentioned above, the mesh convergence analysis was done for different element seed sizes of 0.1, 0.2 and 0.8 mm. As indicated in Table 4, the overall response of the model in terms of initial stiffness and ultimate force was essentially independent of the element size so the seed size of 0.2 mm around the drilled hole was chosen for the numerical study.

4 Discussion

The purpose of this study was to simulate and analyze bone damage occurring at the bone–implant interface in order to

reach a better understanding of the implant primary stability behavior without the need for high-performance computing. The goal was achieved by considering first the implantation process, second by including contact with friction during cyclic loading and finally comparing the overall behavior with respect to an experiment.

For the implantation process, the press-fit was simulated by expanding the initial drilled hole to the outer boundaries of a cylindrical implant. The damaged zone around the implant increased by approximately 50% when increasing the press-fit from the dense to the soft drilling protocol.

This phenomenon has been previously investigated through different approaches. A first approach used high-resolution CT images and strain mapping between images taken before and after implantation. The amount of plastic strain at the interface was calculated and the related damage value assigned. However, it required high-resolution and time-consuming CT imaging techniques and did not deliver the means to predict an outcome for a different degree of press-fit or implant geometry. A second approach modeled the bone as a continuum medium assigning the press-fit configuration to account for the stress induced in the surrounding bone during this process. However, in these studies, the damage was not applied to the material characteristics model and reduction in the material stiffness was not observed (Berahmani et al. 2017). This approach is suitable for small deformations in a linear elastic regime of the surrounding bone but is clearly not adapted for the large amount of press-fit applied for bones with lower BV/TV.

In the progressive loading protocol applied after implantation, the three major aspects of damage, friction and micromotions were studied. Implantation damage was quantified for three different initial press-fit levels corresponding to soft, dense and intact protocols. The intact condition is the main assumption used in the literature for implant loading simulations. As seen in this study, it neglects the reduction in bone stiffness and the densification due to the implantation damage.

In several studies, the bone–implant interface was modeled as fully bonded. This assumption applies to a fully osseointegrated implant surface corresponding de facto to secondary stability. It accounts neither for the observed damage behavior of the bone nor for the sliding occurring between bone and implant and is therefore not suitable for the analysis of primary stability (Maldonado et al. 2003; Dubov et al. 2011; Kennedy et al. 2013). A more recent approach to fully bonded models was conducted with μFE simulations (Steiner et al. 2017a, b). The damage is induced a priori in this model through the reduction in elastic properties in a delimited zone around the implant. This zone and the amount of reduction in elastic properties are determined by the experimental CT images and by fitting the macroscopic stiffness of an experiment, respectively. The problem with this approach is that both the zone and the extent of damage change with implant shape, bone BV/TV, the degree of press-fit and direction of loading. In our study, the fully bonded models with and without the damaged zone have also been simulated and compared with the simulations conducted on different implantation protocols and also the experiment results. It is evident from the results that the fully bonded models have a higher stiffness and ultimate force compared to the no bonded models and illustrate a significant difference with the experiment results when applied to large displacements. In addition, due to lack of damage and plasticity in the model, the unloading behavior and stiffness reduction in further loading steps cannot be captured using these models.

The effect of friction on the bone–implant system response was investigated by changing the friction coefficient between extreme values reported in the literature (Huang et al. 2008; Karunratanakul et al. 2010; MacLeod et al. 2012). Both the initial stiffness and ultimate force increased significantly when changing the friction coefficient from 0.0 to 0.9; however, the rate of this increase vanishes toward the value of 0.9. This is in accordance with the trend observed in numerical results reported by Kelly et al. (2013) for synthetic tibia samples.

The dominant effect of BV/TV on the initial stiffness and ultimate force was also investigated and compared with experimental data. The ultimate force predicted by the simulation matches the experimental trend almost perfectly. However, a slight difference between the experimental and simulation results is observed for initial stiffness. This may be explained by the geometrical approximation and the rigid body assumption for the implant, but also by the increased experimental error in the displacement compared to the force measurements.

In addition, the proposed nonlinear hFE methodology enables quantification of micromotions around the implant, which cannot be achieved by μFE models without contact. The amount of micromotions can first be used to assess primary stability and later used for the evaluation of the healing and osseointegration process leading to secondary stability. According to the micromotions plot obtained for the conducted experiment, the range of micromotions could be investigated and compared with the value of 150 μm reported in the literature for assessing formation of a fibrous tissue layer (Viceconti et al. 2000; Fitzpatrick et al. 2014). In fact, the highest values for micromotions are found at both ends of the implant as the latter tends to rotate with respect to the center portion during the elastic unloading. This approach, in combination with the detailed geometry of the implant, could be used to optimize the implant shape in order to achieve the suitable amount of micromotions.

There are a few limitations to this study. First, the implant geometry was approximated by a cylinder and the implant insertion did not include the vertical and rotational motion

of the real implantation process. The accurate implant geometry was not considered important for an hFE model ignoring also the details of the bone microstructure. Simulation of the real implantation process would require an explicit FE with much higher computational costs and its accurate description was not the scope of our study. The inherent lack of bone microstructure in hFE models is perceived as an advantage when it comes to prediction of the structural response of the bone–implant complex but does obviously not provide any micromechanical results that may be relevant for osseointegration or implant design at the micro level. For the latter purpose, nonlinear μFE models with contact will become necessary. Second, although the hFE model captures the overall mechanical behavior of the experiment quite well, quantitative differences exist. It should be emphasized that no material constant tuning was undertaken. Often drilling of the hole goes slightly beyond the end of the implant, which is likely to reduce the axial stiffness of the bone–implant complex without affecting the maximal force. This may explain the observed differences, but a truly quantitative validation will need to be realized in the future with novel experiments including more realistic heterogeneous bone structures. Moreover, no micromotions and no post-implantation residual forces were obtained by the experiment that could be compared with the computational results. Third, the vertebral trabecular bone was used for inserting dental implants. This may appear awkward, but was motivated by the benefit of available human tissue and justified by the fact that the trabecular bone morphology–mechanical property relations used in hFE do not depend on anatomical location (Gross et al. 2013). The presented qualitative validation is therefore not impaired by this choice.

5 Conclusion

The proposed FE methodology allows investigating the primary stability of the bone–implant complex in terms of initial stiffness, ultimate force and damage for different degrees of implantation press-fit. The goal is achieved by modeling the human trabecular bone as an elasto-plastic material model with damage, whose constants depend on BV/TV and fabric. As micromotions at the bone–implant interface are important for the success of osseointegration, contact with friction is considered for modeling the interface in this approach. The proposed model is able to capture the overall primary stability behavior observed in the experiments despite the limited fidelity of the outer geometry and stiffness of the implant and despite the assumed homogeneity of trabecular bone. The model proves to be more realistic and more time efficient compared to current linear μFE models and will be used in future for investigating the effect of bone heterogeneity on primary stability of different implant designs.

Acknowledgements The authors gratefully acknowledge RMS for their financial support Grant No. E16_0001 HOM-FEM and Nobel Biocare for supporting the realization of the experiments.

Compliance with ethical standards

Conflicts of interest The authors declare that they have no conflicts of interest.

References

Abdul-Kadir MR, Hansen U, Klabunde R, Lucas D, Amis A (2008) Finite element modelling of primary hip stem stability: the effect of interference fit. J Biomech 41(3):587–594. https://doi.org/10.1016/j.jbiomech.2007.10.009

Baggi L, Cappelloni I, Di Girolamo M, Maceri F, Vairo G (2008) The influence of implant diameter and length on stress distribution of osseointegrated implants related to crestal bone geometry: a three-dimensional finite element analysis. J Prosthet Dent 100(6):422–431. https://doi.org/10.1016/S0022-3913(08)60259-0

Basler SE, Traxler J, Müller R, van Lenthe GH (2013) Peri-implant bone microstructure determines dynamic implant cut-out. Med Eng Phys 35(10):1442–1449. https://doi.org/10.1016/j.medengphy.2013.03.016

Berahmani S, Janssen D, Verdonschot N (2017) Experimental and computational analysis of micromotions of an uncemented femoral knee implant using elastic and plastic bone material models. J Biomech 61:137–143. https://doi.org/10.1016/j.jbiomech.2017.07.023

Chappuis V, Engel O, Reyes M, Shahim K, Nolte LP, Buser D (2013) Ridge alterations post-extraction in the esthetic zone. J Dent Res 92(12-suppl):195S–201S. https://doi.org/10.1177/0022034513506713

Charlebois M, Jirásek M, Zysset PK (2010) A nonlocal constitutive model for trabecular bone softening in compression. Biomech Model Mechanobiol 9(5):597–611

Chong DYR, Hansen UN, Amis AA (2010) Analysis of bone-prosthesis interface micromotion for cementless tibial prosthesis fixation and the influence of loading conditions. J Biomech 43(6):1074–1080. https://doi.org/10.1016/j.jbiomech.2009.12.006

Conlisk N, Gray H, Pankaj P, Howie CR (2012) The influence of stem length and fixation on initial femoral component stability in revision total knee replacement. Bone Joint Res 1(11):281–8. https://doi.org/10.1302/2046-3758.111.2000107

Dorogoy A, Rittel D, Shemtov-Yona K, Korabi R (2017) Modeling dental implant insertion. J Mech Behav Biomed Mater 68(January):42–50. https://doi.org/10.1016/j.jmbbm.2017.01.021

Du J, Lee JH, Jang AT, Gu A, Hossaini-Zadeh M, Prevost R, Curtis DA, Ho SP (2015) Biomechanics and strain mapping in bone as related to immediately-loaded dental implants. J Biomech 48(12):3486–3494. https://doi.org/10.1016/j.jbiomech.2015.05.014

Dubov A, Kim SYR, Shah S, Schemitsch EH, Zdero R, Bougherara H (2011) The biomechanics of plate repair of periprosthetic femur fractures near the tip of a total hip implant: the effect of cable-screw position. Proc Inst Mech Eng 225(9):857–865

Fitzpatrick CK, Hemelaar P, Taylor M (2014) Computationally efficient prediction of bone-implant interface micromotion of a cementless tibial tray during gait. J Biomech 47(7):1718–1726. https://doi.org/10.1016/j.jbiomech.2014.02.018

Fouad H (2010) Effects of the bone-plate material and the presence of a gap between the fractured bone and plate on the predicted stresses at the fractured bone. Med Eng Phys 32(7):783–789. https://doi.org/10.1016/j.medengphy.2010.05.003

Gabet Y, Kohavi D, Voide R, Mueller TL, Müller R, Bab I (2010) Endosseous implant anchorage is critically dependent on mechanostructural determinants of peri-implant bone trabeculae. J Bone Miner Res 25(3):575–583. https://doi.org/10.1359/jbmr.090808

Gapski R, Wang HL, Mascarenhas P, Lang NP (2003) Critical review of immediate implant loading. Clin Oral Implant Res 14(5):515–527. https://doi.org/10.1034/j.1600-0501.2003.00950.x

Gross T, Pahr DH, Zysset PK (2013) Morphology–elasticity relationships using decreasing fabric information of human trabecular bone from three major anatomical locations. Biomech Model Mechanobiol 12(4):793–800. https://doi.org/10.1007/s10237-012-0443-2

Haïat G, Hl Wang, Brunski J (2014) Effects of biomechanical properties of the bone implant interface on dental implant stability: from in silico approaches to the patient's mouth. Annu Rev Biomed Eng 16(1):187–213. https://doi.org/10.1146/annurev-bioeng-071813-104854

Hosseini HS, Pahr DH, Zysset PK (2012) Modeling and experimental validation of trabecular bone damage, softening and densification under large compressive strains. J Mech Behav Biomed Mater 15:93–102

Hosseini HS, Clouthier AL, Zysset PK (2014) Experimental validation of finite element analysis of human vertebral collapse under large compressive strains. J Biomech Eng 136(4):41,006

Hosseini HS, Horák M, Zysset PK, Jirásek M (2015) An over-nonlocal implicit gradient-enhanced damage-plastic model for trabecular bone under large compressive strains. Int J Numer Methods Biomed Eng 31(11):e02728

Huang HL, Hsu JT, Fuh LJ, Tu MG, Ko CC, Shen YW (2008) Bone stress and interfacial sliding analysis of implant designs on an immediately loaded maxillary implant: a non-linear finite element study. J Dent 36(6):409–417. https://doi.org/10.1016/j.jdent.2008.02.015

Inzana JA, Varga P, Windolf M (2016) Implicit modeling of screw threads for efficient finite element analysis of complex bone-implant systems. J Biomech 49(9):1836–1844. https://doi.org/10.1016/j.jbiomech.2016.04.021

Karunratanakul K, Schrooten J, Van Oosterwyck H (2010) Finite element modelling of a unilateral fixator for bone reconstruction: importance of contact settings. Med Eng Phys 32(5):461–467. https://doi.org/10.1016/j.medengphy.2010.03.005

Kelly N, Cawley DT, Shannon FJ, Mcgarry JP (2013) Medical engineering & physics an investigation of the inelastic behaviour of trabecular bone during the press-fit implantation of a tibial component in total knee arthroplasty. Med Eng Phys 35(11):1599–1606. https://doi.org/10.1016/j.medengphy.2013.05.007

Kennedy J, Molony D, Burke NG, FitzPatrick D, Mullett H (2013) Effect of calcium triphosphate cement on proximal humeral fracture osteosynthesis: a cadaveric biomechanical study. J Orthop Surg 21(2):173–177. https://doi.org/10.1177/230949901302100211

Korabi R, Shemtov-Yona K, Rittel D (2017) On stress/strain shielding and the material stiffness paradigm for dental implants. Clin Implant Dent Relat Res 19:935–943. https://doi.org/10.1111/cid.12509

Lioubavina-Hack N, Lang NP, Karring T (2006) Significance of primary stability for osseointegration of dental implants. Clin Oral Implant Res 17(3):244–250. https://doi.org/10.1111/j.1600-0501.2005.01201.x

MacLeod AR, Pankaj P, Simpson AHR (2012) Does screw-bone interface modelling matter in finite element analyses? J Biomech 45(9):1712–1716. https://doi.org/10.1016/j.jbiomech.2012.04.008

Maldonado ZM, Seebeck J, Heller MOW, Brandt D, Hepp P, Lill H, Duda GN (2003) Straining of the intact and fractured proximal humerus under physiological-like loading. J Biomech 36(12):1865–1873

Meredith N (2008) A review of implant design, geometry and placement. Appl Osseointgrated Res 6:6–12

Mueller TL, Basler SE, Müller R, Van Lenthe GH (2013) Time-lapsed imaging of implant fixation failure in human femoral heads. Med Eng Phys 35(5):636–643. https://doi.org/10.1016/j.medengphy.2012.07.009

Pankaj P (2013) Patient-specific modelling of bone and bone-implant systems: the challenges. Int J Numer Method Biomed Eng. https://doi.org/10.1002/cnm.2536

Panyasantisuk J, Pahr DH, Zysset PK (2016) Effect of boundary conditions on yield properties of human femoral trabecular bone. Biomech Model Mechanobiol 15(5):1043–1053. https://doi.org/10.1007/s10237-015-0741-6

Ruffoni D, Müller R, Van Lenthe GH (2012) Mechanisms of reduced implant stability in osteoporotic bone. Biomech Model Mechanobiol 11(3–4):313–323. https://doi.org/10.1007/s10237-011-0312-4

Schwiedrzik JJ, Wolfram U, Zysset PK (2013) A generalized anisotropic quadric yield criterion and its application to bone tissue at multiple length scales. Biomech Model Mechanobiol 12(6):1155–1168

Steiner JA, Ferguson SJ, van Lenthe GH (2015) Computational analysis of primary implant stability in trabecular bone. J Biomech 48(5):807–815. https://doi.org/10.1016/j.jbiomech.2014.12.008

Steiner JA, Ferguson SJ, van Lenthe GH (2016) Screw insertion in trabecular bone causes peri-implant bone damage. Med Eng Phys 38(4):417–422. https://doi.org/10.1016/j.medengphy.2016.01.006

Steiner JA, Christen P, Affentranger R, Ferguson SJ, van Lenthe GH (2017a) A novel in silico method to quantify primary stability of screws in trabecular bone. J Orthop Res. https://doi.org/10.1002/jor.23551

Steiner JA, Hofmann UA, Christen P, Favre JM, Ferguson SJ, van Lenthe GH (2017b) Patient-specific in silico models can quantify primary implant stability in elderly human bone. J Orthop Res. https://doi.org/10.1002/jor.23721

van Rietbergen B, Weinans H, Huiskes R, Odgaard A (1995) A new method to determine trabecular bone elastic properties and loading using micromechanical finite-element models. J Biomech 28(1):69–81. https://doi.org/10.1016/0021-9290(95)80008-5

Varga P, Grünwald L, Inzana JA, Windolf M (2017) Fatigue failure of plated osteoporotic proximal humerus fractures is predicted by the strain around the proximal screws. J Mech Behav Biomed Mater 75:68–74. https://doi.org/10.1016/j.jmbbm.2017.07.004

Viceconti M, Muccini R, Bernakiewicz M, Baleani M, Cristofolini L (2000) Large-sliding contact elements accurately predict levels of bone-implant micromotion relevant to osseointegration. J Biomech 33(12):1611–1618. https://doi.org/10.1016/S0021-9290(00)00140-8

Wolfram U, Wilke HJ, Zysset PK (2011) Damage accumulation in vertebral trabecular bone depends on loading mode and direction. J Biomech 44(6):1164–1169. https://doi.org/10.1016/j.jbiomech.2011.01.018

Zhang QH, Tan SH, Chou SM (2004) Investigation of fixation screw pull-out strength on human spine. J Biomech 37(4):479–485. https://doi.org/10.1016/j.jbiomech.2003.09.005

Publisher's Note Springer Nature remains neutral with regard to jurisdictional claims in published maps and institutional affiliations.